SUPPLEMENTAL FIGURE

Kv3.3 channels harboring a mutation of spinocerebellar ataxia type 13 alter excitability and induce cell death in cultured cerebellar Purkinje cells

Tomohiko Irie, Yasunori Matsuzaki, Yuko Sekino, and Hirokazu Hirai

Supplemental Fig. S1

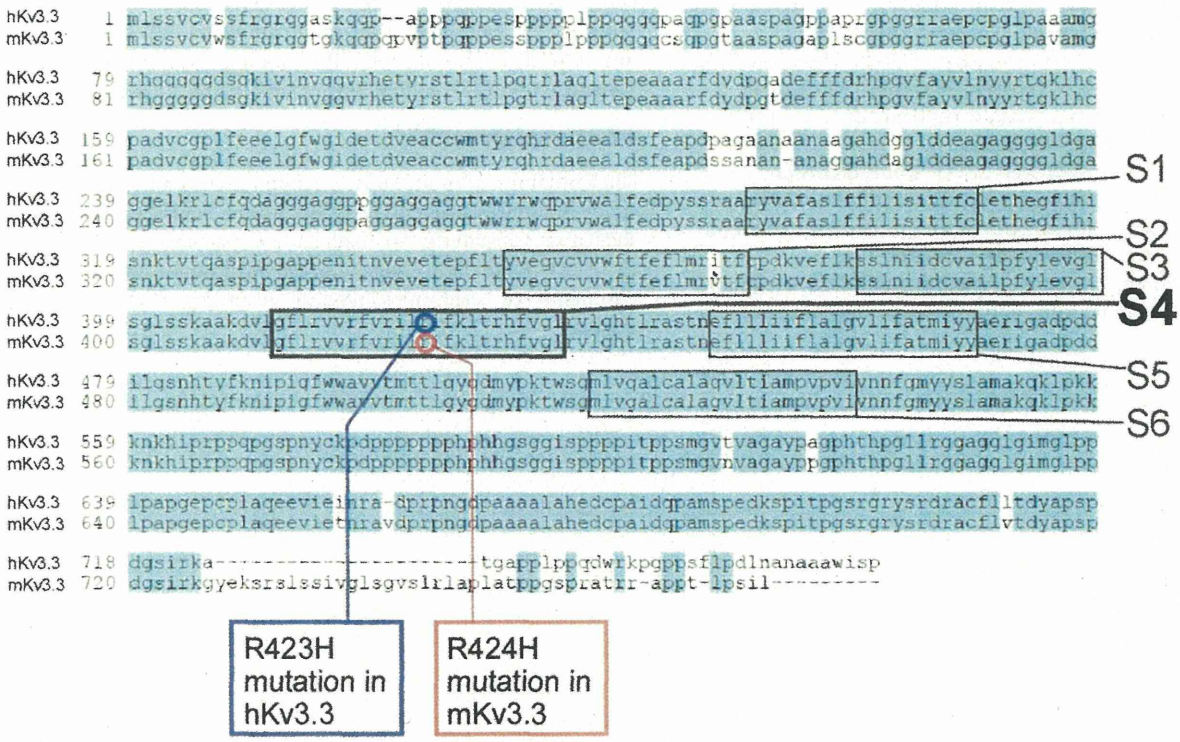

Supplemental Figure S1. Amino acid sequence alignment of hKv3.3 (accession number AF022150) with the mKv3.3 used in this experiment

The two sequences were aligned using Clone Manager 6 software (Scientific & Educational Software, Cary, NC). Hyphens represent gaps introduced to optimize the alignment. The six transmembrane domains are surrounded by squares. Residues conserved between hKv3.3 and mKv3.3 are colored blue.

Supplemental Fig. S2

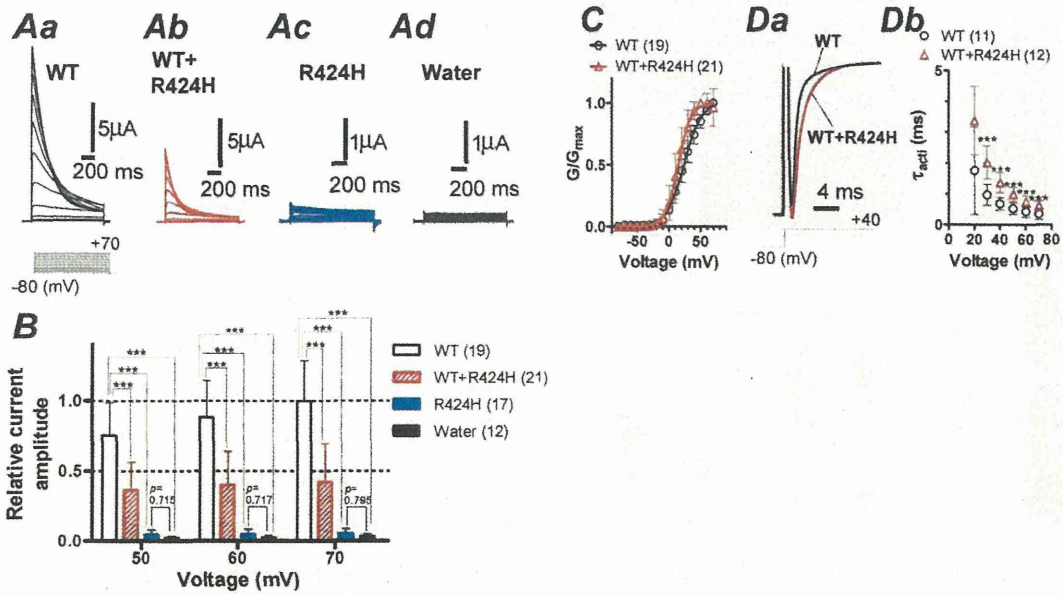

Supplemental Figure S2. R424H mutant subunits work as a dominant-negative on WT mKv3.3 channels expressed in *Xenopus* oocytes

A, Representative traces evoked by stepping from −80 mV holding potential to voltages ranging from −70 to +70 mV in 10-mV increments. cRNA of WT mKv3.3 (*Aa*, WT), a mixture of WT and R424H mutant subunits at 1:1 ratio (*Ab*, WT+R424H), R424H mutant subunits (*Ac*, R424H), or nuclease-free water (*Ad*, Water) was injected into *Xenopus* oocytes. *B*, Summary of the mean relative current amplitude. The amplitude was calculated from peak amplitude normalized by mean peak amplitude of WT-expressing oocytes at +70 mV voltage pulse. *C*, Normalized conductance (*G*) of WT-expressing and WT+R424H-expressing oocytes are plotted as a function of voltage. *G* was obtained by dividing peak current by electrochemical driving force: $[G = I_K/(V - E_K)]$. The activation (G/G_{max}) curves were fit with the Boltzmann function, $G/G_{max} = 1/ [1 + \exp (V_{1/2} - V)/k]$. *D*, Comparison of activation τ between WT-expressing and WT+R424H mutant-expressing oocytes. *Da*, Representative traces evoked by stepping from −80 mV holding potential to +40 mV. The current traces are scaled to the same peak amplitude to compare the activation kinetics. *Db*, Comparison of τ_{acti} of WT mKv3.3 with that of WT+R424H mutant channels in *Xenopus* oocytes. τ_{acti} was obtained by fitting current traces with a single exponential function on the rising phases of the traces.

Supplemental Fig. S3

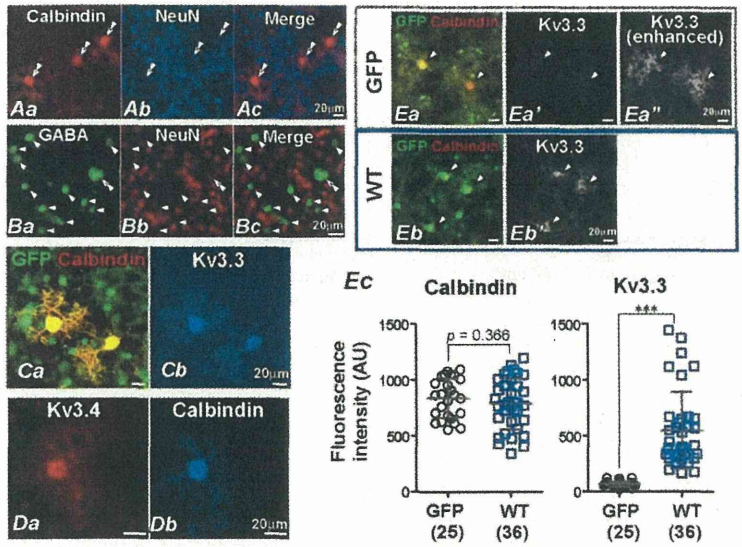

Supplemental Figure S3. Immunohistochemical characterization of mouse cerebellar cultures

A, Cerebellar cultures double-immunostained with anti-Calbindin and anti-NeuN antibodies at DIV 14. PCs (Calbindin-positive cells in *Aa*, double arrowheads) were NeuN-negative (*Ab* and *Ac*). *B*, Cultures double-immunostained with anti-GABA and anti-NeuN antibodies at DIV 16. GABAergic interneurons (GABA-positive small cells in *Ba* and *Bc*, arrowheads) were also NeuN-negative. Double arrowheads in *Ba* and *Bc* indicate a putative PC. *C*, Cultures triple-immunostained with anti-GFP, anti-Calbindin, and anti-Kv3.3 antibodies at DIV 14. PCs but not other cerebellar neurons expressed mKv3.3 channels. In *C*, GFP-expressing cerebellar cultures were used to visualize the neurons. *D*, Cerebellar cultures double-immunostained with anti-Kv3.4 and anti-Calbindin antibodies, showing the expression of Kv3.4 in PCs. *E*, Immunofluorescence images of cerebellar cultures infected with lentiviral vectors expressing GFP (*Ea-Ea"*) or WT subunits (*Eb* and *Eb'*). The cultures were double-immunostained with anti-GFP and anti-Kv3.3 antibodies. The fluorescence images were taken in the same conditions for the quantitative analysis. PCs are indicated by arrowheads. Panel *Ea"* is a contrast-enhanced image of *Ea'* that shows faint but some expression of endogenous mKv3.3 in PCs expressing GFP alone. *Ec*, Quantitative analysis of immunofluorescence intensity for Calbindin and Kv3.3. AU, arbitrary unit. In *A-E*, The following primary and secondary antibodies were used. Primary antibodies: mouse monoclonal anti-Calbindin antibody (*A*, *C*, and *D*, 1:2,000-diluted, No.300, Swant; Bellinzona, Switzerland), mouse monoclonal anti-NeuN antibody (*A* and *B*, 1:2,000-diluted), and rabbit polyclonal anti-GABA antibody (*B*, 1:1,000-diluted, A2052; Sigma-Aldrich), guinea pig polyclonal anti-GFP antibody (*C* and *E*, 1:1,000-diluted), and rabbit polyclonal anti-Kv3.3 antibody [*C* and *E*, 1:2,000-diluted, APC-102; Alomone labs, Jerusalem, Israel; This antibody is raised from the peptide KSPITPGSRGRYSRDRAC corresponding with residues 701-718 of rat Kv3.3a channels, which have a sequence that is identical to 692-709 of the mKv3.3 channels (Chang *et al.*, 2007)]. Secondary antibodies: AF 568-conjugated goat anti-rabbit IgG antibody (3*A*), AF 680-conjugated goat anti-mouse IgG antibody (*A* and *D*), AF 488-conjugated goat anti-rabbit IgG antibody (*B*, A-11008; Invitrogen), AF 568-conjugated goat anti-mouse IgG antibody (*B*, *C* , and *E*, A-11031; Invitrogen), AF 488-conjugated goat anti-guinea pig IgG antibody (*C* and *E*), AF 680-conjugated goat anti-rabbit IgG antibody (*C* and *E*, A-21109; Invitrogen). All secondary antibodies were used at the concentration of 5 μg/ml. The incubation conditions were same as Fig. 2. For immunolabeling of Kv3.4 protein in cerebellar cultures (*D*), goat serum was excluded from the incubation buffer. Cerebellar cultures were immunolabeled with goat polyclonal anti-hKv3.4 antibody (1:500-diluted, sc-104343; Santa Cruz Biotechnology, Santa Cruz, CA) and mouse monoclonal anti-Calbindin antibody, and then with AF 568-conjugated donkey anti-goat IgG antibody (A-11057; Invitrogen). After blocking with the incubation buffer containing 10% normal goat serum, the cultures were further incubated with AF 680-conjugated goat anti-mouse IgG antibody.

Supplemental Fig. S4

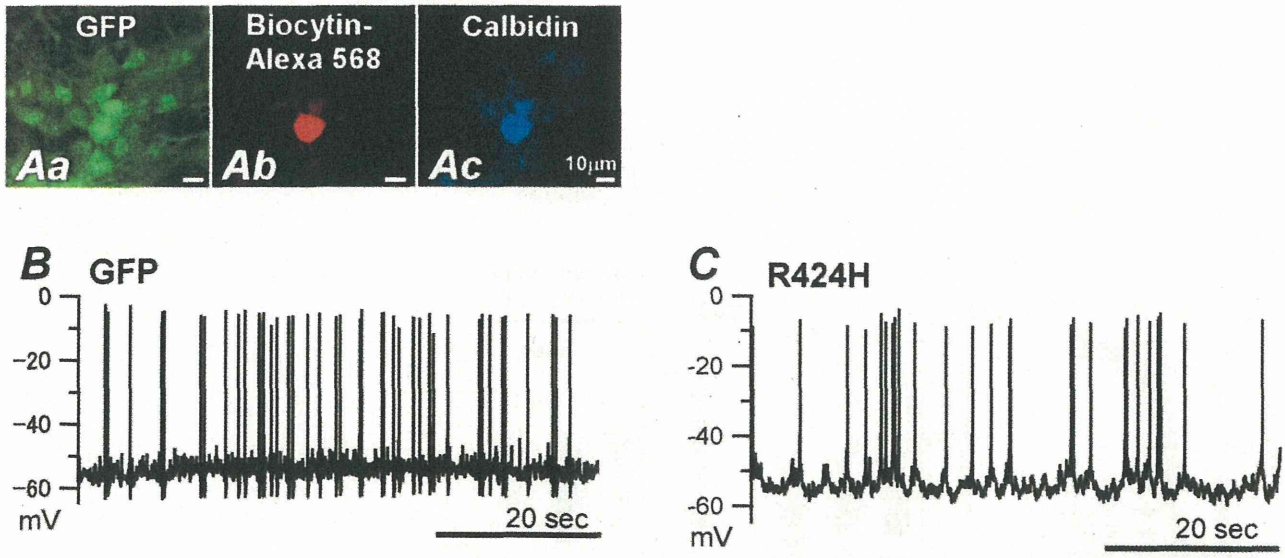

Supplemental Figure S4. Recordings of spontaneous action potentials from PCs

A, Immunohistochemical identification of PCs. PCs were stained intracellularly with biocytin infused via patch pipettes, fixed in 4% (w/v) formaldehyde, and incubated with mouse monoclonal anti-Calbindin antibody and guinea pig polyclonal anti-GFP antibody. The samples were further incubated with AF 568 streptavidin (S-11226, Invitrogen), AF 488-conjugated goat anti-guinea pig IgG antibody, and AF 680-conjugated goat anti-mouse IgG antibody. The incubation conditions were the same as in Fig. 2. *B* and *C*, Representative spontaneous firing recorded from GFP-expressing PC (*B*) and R424H mutant-expressing PC (*C*) at DIV 8.

Supplemental Fig. S5

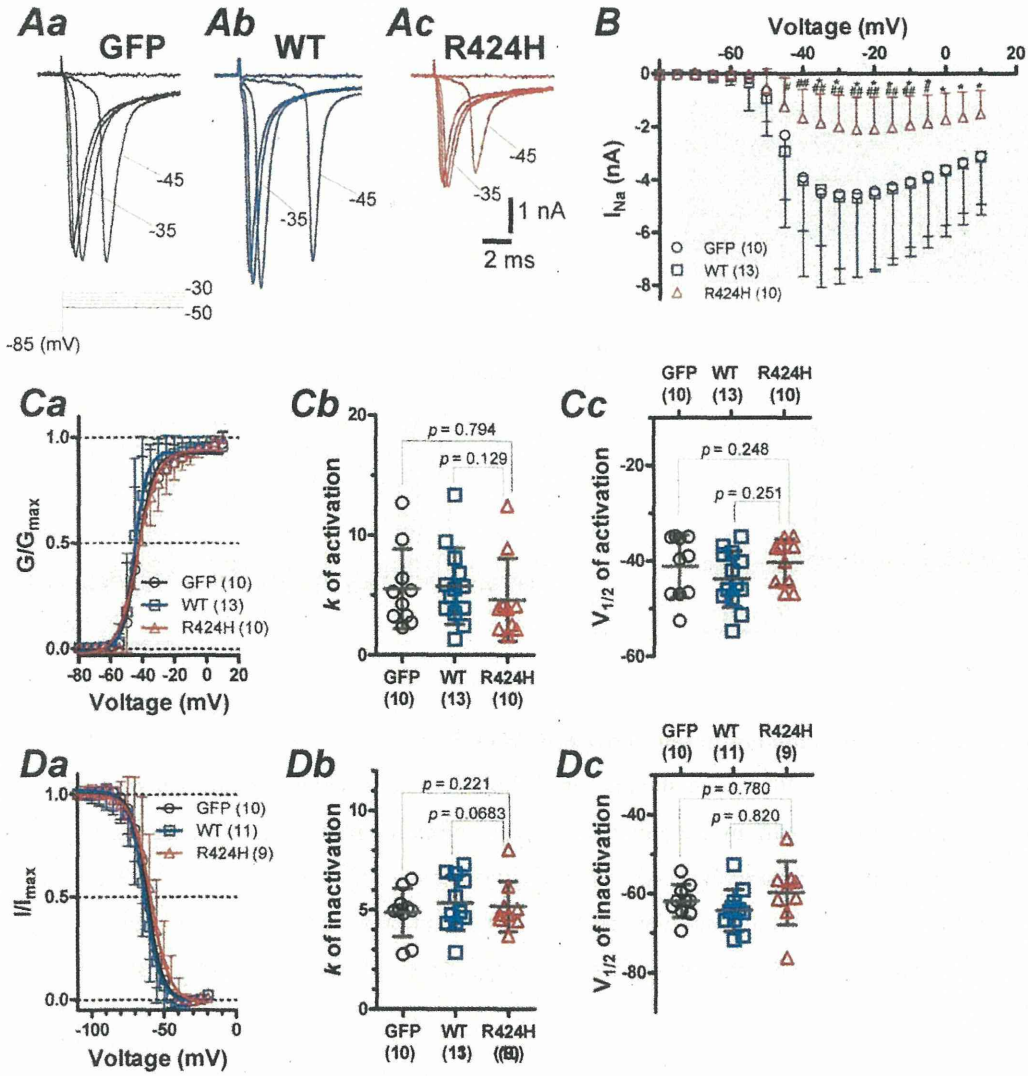

Supplemental Figure S5. Comparison of I_{Na} recorded under the whole-cell configuration

I_{Na} was recorded in HEPES-buffered ACSF in which 140 NaCl (in mM) was replaced with 117 NaCl, 22 TEA-Cl, 3 CsCl, and 2 4-aminopyridine, 0.2 $CdCl_2$, 0.1 picrotoxin, and 0.02 DNQX; RT (20-22°C). A CsCl-based internal solution was used (in mM): 140 CsCl, 10 NaCl, 0.2 EGTA, 10 biocytin, and 10 HEPES (pH 7.3 with CsOH, E_{Na} = 63.4 mV). The liquid junction potential (−5 mV) was corrected off-line. *A*, Representative traces of I_{Na} activated with 50-ms voltage steps from −85 mV to voltages ranging from −50 to −30 mV in 5-mV increments. The leak currents were subtracted on-line the p/4 protocol and the I_{Na} was confirmed by application of TTX (0.001 mM, data not shown). *B*, The current-voltage relation of peak I_{Na}. In this figure, an asterisk (*) indicates statistical significance between GFP alone and R424H mutant, and a number sign (#) between WT mKv3.3 and R424H. *p < 0.05, #p < 0.05, and ##p < 0.01. *Ca*, The conductance-voltage relations, which were obtained in the same way as those in Supplemental Fig. S2*C*. E_{Na} was used for the equilibrium potential. *Cb* and *Cc*, k (*Cb*) and $V_{1/2}$ (*Cc*) of activation for R424H mutant-expressing PCs did not show significant difference compared to those for the control group. *D*, The steady-state inactivation was determined by holding cells at −85 mV before applying a 200-ms pre-pulse to potentials between −125 and −20 mV in 5-mV increments, followed by a 100-ms test pulse to −20 mV. *Da*, Steady-state inactivation curves were obtained in the same way as those in Fig. 1*Bc*. *Db* and *Dc*, k (*Db*) and $V_{1/2}$ (*Dc*) for R424H mutant-expressing PCs did not show significant difference compared to those for the control group.

The Journal of Toxicological Sciences (J. Toxicol. Sci.)
Vol.39, No.2, 285-292, 2014

Toxicomics Report

Proteomic analysis of ethanol-induced embryotoxicity in cultured post-implantation rat embryos

Makoto Usami[1], Katsuyoshi Mitsunaga[2], Tomohiko Irie[1], Atsuko Miyajima[3] and Osamu Doi[4]

[1]*Division of Pharmacology, National Institute of Health Sciences, 1-18-1 Kamiyoga, Setagaya, Tokyo, 158-8501, Japan*
[2]*School of Pharmaceutical Sciences, Toho University, 2-2-1 Miyama, Funabshi, Chiba, 274-8510, Japan*
[3]*Division of Medical Devices, National Institute of Health Sciences, 1-18-1 Kamiyoga, Setagaya, Tokyo, 158-8501, Japan*
[4]*Laboratory of Animal Reproduction, United Graduate School of Agricultural Science, Gifu University, 1-1 Yanagido, Gifu, 501-1193, Japan*

(Received November 9, 2013; Accepted December 18, 2013)

ABSTRACT — Protein expression changes were examined in day 10.5 rat embryos cultured for 24 hr in the presence of ethanol by using two-dimensional electrophoresis and mass spectrometry. Exposure to ethanol resulted in quantitative changes in many embryonic protein spots (16 decreased and 28 increased) at *in vitro* embryotoxic concentrations (130 and 195 mM); most changes occurred in a concentration-dependent manner. For these protein spots, 17 proteins were identified, including protein disulfide isomerase A3, alpha-fetoprotein, phosphorylated cofilin-1, and serum albumin. From the gene ontology classification and pathway mapping of the identified proteins, it was found that ethanol affected several biological processes involving oxidative stress and retinoid metabolism.

Key words: Ethanol, Embryotoxicity, Proteomics, Rat

INTRODUCTION

Developmental toxicology is a rapidly growing area of proteomics; it is expected to provide mechanistic insights and protein biomarkers for the safety evaluation of chemicals (Usami and Mitsunaga, 2011). For example, expression changes in actin-binding proteins were considered to be involved in selenate embryotoxicity in the rat whole embryo culture (Usami *et al.*, 2008). Differences in strain sensitivity to cadmium-induced teratogenicity were related to unfolded protein response process and actin polymerization in the mouse limb-bud culture (Chen *et al.*, 2008). Furthermore, based on cluster analysis of proteins with expression changes in the embryonic stem cell test, chemicals were classified into highly embryotoxic and non- or weakly embryotoxic (Groebe *et al.*, 2010). It is thus important to accumulate proteomic analysis data in the field of developmental toxicology. In the present study, protein expression changes in day 10.5 rat embryos cultured for 24 hr in the presence of ethanol, a well-known developmental toxicant, were examined by two-dimensional electrophoresis (2-DE) and mass spectrometry (MS).

MATERIAL AND METHODS

Embryo culture and ethanol treatment

Day 10.5 embryos (plug day = day 0.5) of Wistar rats (Crlj: WI, Charles River Laboratories Japan, Inc., Kanagawa, Japan) were cultured for 24 hr (Usami *et al.*, 2008). Ethanol was diluted in Hank's balanced salt solution in two-fold and added to the culture medium composed of 100% rat serum at concentrations of 0, 65, 130, and 195 mM. Medium-sized cultured embryos (four embryos per treatment group) were selected for subsequent protein analyses. All animal experiments were carried out according to the guidelines for animal use of the National Institute of Health Sciences.

2-DE and MS analyses of embryonic protein

The analyses of 2-DE gels (one embryo per gel, four gels per treatment group) were carried out as previously reported (Usami *et al.*, 2009), except that the gels were stained with a fluorescent dye (Flamingo gel stain, Bio-Rad, Hercules, CA, USA) and scanned with a laser scanner (FLA-5100, GE Healthcare UK Ltd., Amersham Place, Little Chalfont, UK) at an excitation wavelength of

Correspondence: Makoto Usami (E-mail: usami@nihs.go.jp)

473 nm. Quantitative differences in protein spots of more than 1.5-fold with statistical significance by the *t*-test at 5% probability level between the control and 195 mM ethanol groups, were regarded as ethanol-induced protein expression changes.

Classification and mapping of identified proteins

NCBInr GI numbers of the identified proteins were mapped to UniProtKB AC, and gene ontology (GO) terms were assigned using the UniProt web site (http://www.uniprot.org/) (Jain *et al.*, 2009; The UniProt Consortium, 2011). The occurrence of the GO terms (76 biological processes) of the proteins was counted with the CateGOrizer web tool in the "MGI_GO_slim2" ancestor terms using the multiple count method (http://www.animalgenome.org/tools/catego/) (Hu *et al.*, 2008). UniProtKB ACs of the proteins were queried against the KEGG PATHWAY for *Rattus norvegicus* with the KEGG Mapper on the GenomeNet web site (http://www.genome.jp/en/).

RESULTS

Effects of ethanol on the growth of cultured rat embryos

Ethanol inhibited the growth of cultured embryos at concentrations of 130 mM or higher in a concentration-dependent manner (Table 1). Deformed organs included branchial arch, heart, neural tube, optic vesicle, otic vesicle, somite, and tail (Fig. 1), which is in agreement with previous reports (Giavini *et al.*, 1992; Zhou *et al.*, 2011). Compared to blood ethanol levels found in humans, these embryotoxic ethanol concentrations are rather high; however, an ethanol concentration of 150 mM can be observed after acute alcohol intake in chronic alcoholics and 200 mM of ethanol has often been used in *in vitro* toxicological experiments (Li and Kim, 2003; Szabo *et al.*, 1994; Wentzel and Eriksson, 2008).

Effects of ethanol on embryonic protein expression

About 900 protein spots were matched through sixteen 2-DE gels (four gels per experimental group). Quality changes, i.e., appearance or disappearance, in the

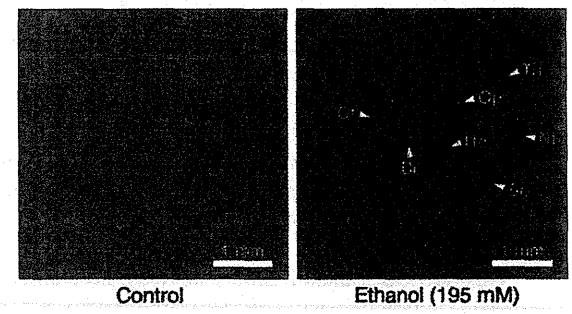

Fig. 1. Appearance of rat embryos cultured in the presence of ethanol. Rat embryos at the end of 24-hr culture are shown after removal of the embryonic membranes. Arrowheads indicate deformed organs. Br, branchial arch; He, heart; Nt, neural tube; Op, optic vesicle; Ot, otic vesicle; So, somite; Ta, tail.

Table 1. Growth of day 10.5 rat embryos cultured in the presence of ethanol

	Ethanol (mM)			
	0 (Control)	65	130	195
No. of embryos	6	5	6	5
No. of viable embryos	6 (100%)	5.(100%)	6 (100%)	5 (100%)
Crown-rump length (mm)	4.11 ± 0.15	3.99 ± 0.17	3.72 ± 0.29*	3.25 ± 0.28**
Head length (mm)	2.23 ± 0.11	2.16 ± 0.14	2.01 ± 0.22	1.74 ± 0.35**
No. of somite pairs	26.7 ± 0.52	26.4 ± 0.55	24.5 ± 2.81	21.2 ± 2.49**
No. of embryos with deformed organ	0	0	3 (50%)	5 (100%)**
Branchial arch	0	0	2 (33%)	4 (80%)*
Heart	0	0	1 (17%)	3 (60%)
Neural tube	0	0	2 (33%)	2 (40%)
Optic vesicle	0	0	2 (33%)	5 (100%)**
Otic vesicle	0	0	2 (33%)	5 (100%)**
Somite	0	0	3 (50%)	5 (100%)**
Tail	0	0	2 (33%)	4 (80%)*

Embryos were cultured for 24 hr by the roller method. Asterisks indicate statistically significant differences compared to the control group identified by Dunnett's multiple comparison test or Fisher's exact test (* $p < 0.05$; ** $p < 0.01$).

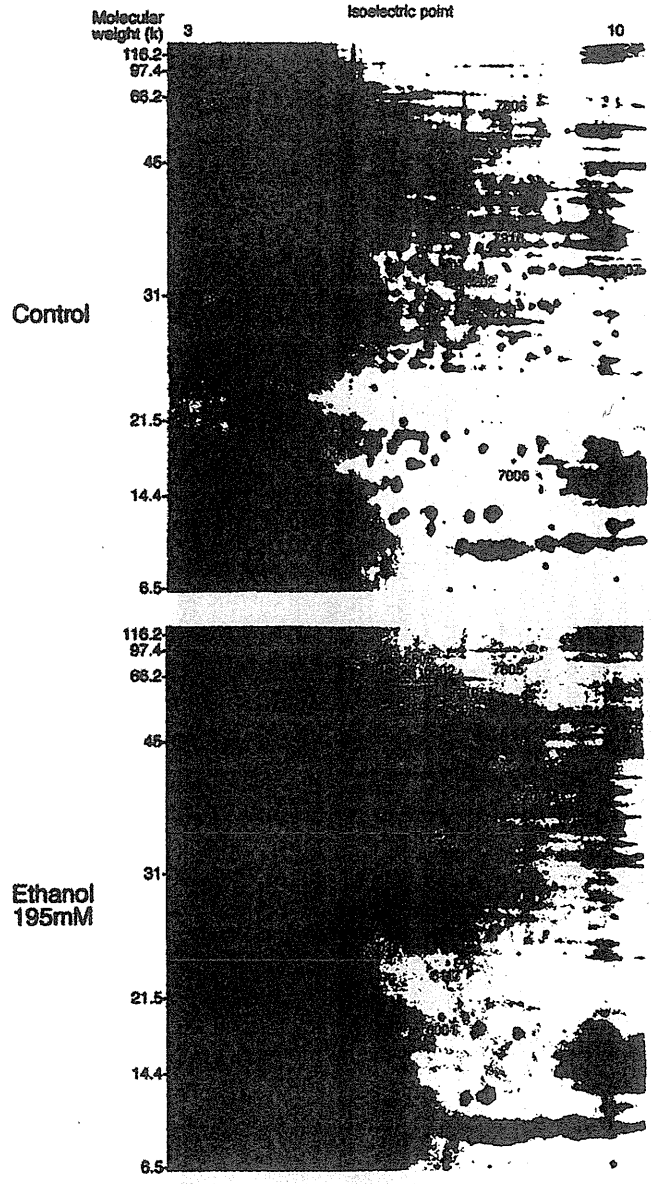

Fig. 2. Two-dimensional electrophoresis pattern of proteins from rat embryos cultured in the presence of ethanol. Representative gels are shown for the control and ethanol (195 mM) groups. Proteins with ethanol-induced expression changes are indicated by circles with standard spot numbers (SSPs); decreased proteins are indicated in the "control" gel (top) and increased ones in the "ethanol" gel (bottom).

protein spots were not observed. Ethanol-induced quantitative changes were noted in 44 spots, i.e., 16 spots were decreased and 28 spots were increased by 1.5-fold or more. The differences between the 195 mM ethanol group and the control group were significant and occurred for most proteins in a concentration-dependent manner (Figs. 2 and 3). Of these spots, 23 were analyzed by MS, resulting in the identification of 7 proteins that were decreased (Table 2) and 11 proteins that were increased (Table 3). Some proteins that were increased, e.g., alpha-fetopro-

Table 2. Proteins whose expression was decreased and their GO terms identified by two-dimensional electrophoresis analysis of rat embryos cultured in the presence of ethanol

SSP	Protein Name	UniProtKB AC	GO term for Biological Process
0505	Protein SET	Q63945	GO:0006334 nucleosome assembly
0601	Nucleosome assembly protein 1-like 1	Q9Z2G8	GO:0006334 nucleosome assembly
0817	Myristoylated alanine-rich C-kinase substrate	P30009	n.a.
1802	78 kDa glucose-regulated protein	P06761	GO:0006916 anti-apoptosis GO:0006983 ER overload response GO:0006987 activation of signaling protein activity involved in unfolded protein response GO:0021589 cerebellum structural organization GO:0021680 cerebellar Purkinje cell layer development GO:0030512 negative regulation of transforming growth factor beta receptor signaling pathway GO:0031398 positive regulation of protein ubiquitination GO:0042149 cellular response to glucose starvation GO:0043066 negative regulation of apoptotic process GO:0043154 negative regulation of cysteine-type endopeptidase activity involved in apoptotic process GO:0051603 proteolysis involved in cellular protein catabolic process
1813	Heat shock cognate 71 kDa protein	P63018	GO:0006351 transcription, DNA-dependent GO:0006355 regulation of transcription, DNA-dependent GO:0006950 response to stress GO:0045892 negative regulation of transcription, DNA-dependent GO:0051085 chaperone mediated protein folding requiring cofactor GO:0061077 chaperone-mediated protein folding
2011	Uncharacterized protein	D3ZRS6	n.a.
4714	Protein disulfide-isomerase A3	P11598	GO:0006662 glycerol ether metabolic process GO:0043065 positive regulation of apoptotic process GO:0045454 cell redox homeostasis

n.a., not available.

Table 3. Proteins whose expression was increased and their GO terms identified by two-dimensional electrophoresis analysis of rat embryos cultured in the presence of ethanol

SSP	Protein Name	UniProtKB AC	GO term for Biological Process
2103	Myosin light chain 3	P16409	GO:0002026 regulation of the force of heart contraction GO:0006936 muscle contraction GO:0006942 regulation of striated muscle contraction GO:0007519 skeletal muscle tissue development GO:0055010 ventricular cardiac muscle tissue morphogenesis GO:0060048 cardiac muscle contraction
2512	BWK4 AND Eukaryotic initiation factor 4A-II OR Eukaryotic translation initiation factor 4A1	Q5VLR5 AND Q5RKI1 OR Q6P3V8	GO:0006457 protein folding AND GO:0006950 response to stress GO:0006986 response to unfolded protein GO:0009100 glycoprotein metabolic process GO:0045454 cell redox homeostasis AND GO:0006413 translational initiation

3509	Eukaryotic translation initiation factor 4A1	Q6P3V8	GO:0006413 translational initiation
4009	Fatty acid-binding protein	P07483	GO:0006631 fatty acid metabolic process GO:0006635 fatty acid beta-oxidation GO:0006656 phosphatidylcholine biosynthetic process GO:0006810 transport GO:0015909 long-chain fatty acid transport GO:0032868 response to insulin stimulus GO:0042493 response to drug GO:0070542 response to fatty acid
5001	Adenine phosphoribosyltransferase	P36972	GO:0006166 purine ribonucleoside salvage GO:0006168 adenine salvage GO:0007595 lactation GO:0009116 nucleoside metabolic process GO:0032869 cellular response to insulin stimulus
6001	Cofilin-1	P45592	GO:0006606 protein import into nucleus GO:0007010 cytoskeleton organization GO:0022604 regulation of cell morphogenesis GO:0030030 cell projection organization GO:0045792 negative regulation of cell size
6516	Elongation factor 1-gamma	Q68FR6	GO:0006412 translation GO:0006414 translational elongation
4727 5702 5710 5716 6601	Protein disulfide-isomerase A3	P11598	GO:0006662 glycerol ether metabolic process GO:0043065 positive regulation of apoptotic process GO:0045454 cell redox homeostasis
4810 4818	Alpha-fetoprotein	P02773	GO:0001542 ovulation from ovarian follicle GO:0001889 liver development GO:0006810 transport GO:0010033 response to organic substance GO:0019953 sexual reproduction GO:0031016 pancreas development GO:0031100 organ regeneration GO:0042448 progesterone metabolic process GO:0060395 SMAD protein signal transduction
4832 5805 6802	Serum albumin	P02770	GO:0006810 transport GO:0006950 response to stress GO:0007584 response to nutrient GO:0009267 cellular response to starvation GO:0010033 response to organic substance GO:0019836 hemolysis by symbiont of host erythrocytes GO:0042311 vasodilation GO:0043066 negative regulation of apoptotic process GO:0046010 positive regulation of circadian sleep/wake cycle, non-REM sleep GO:0046689 response to mercury ion GO:0051659 maintenance of mitochondrion location GO:0070541 response to platinum ion

SSP 2512 contained two proteins.

Table 4. KEGG pathway mapping of proteins identified by two-dimensional electrophoresis analysis of rat embryos cultured in the presence of ethanol

Pathway ID	Pathway name	UniProtKB AC	Protein Name (Total number of mapped pathways)
rno04612	Antigen processing and presentation	P06761	78 kDa glucose-regulated protein (4)
		P11598	Protein disulfide-isomerase A3 (2)
		P63018	Heat shock cognate 71 kDa protein (9)
rno04141	Protein processing in endoplasmic reticulum	P06761	78 kDa glucose-regulated protein (4)
		P11598	Protein disulfide-isomerase A3 (2)
		P63018	Heat shock cognate 71 kDa protein (9)
rno05134	Legionellosis	P63018	Heat shock cognate 71 kDa protein (9)
		Q68FR6	Elongation factor 1-gamma (1)
rno03040	Spliceosome	P63018	Heat shock cognate 71 kDa protein (9)
rno04010	MAPK signaling pathway	P63018	Heat shock cognate 71 kDa protein (9)
rno04144	Endocytosis	P63018	Heat shock cognate 71 kDa protein (9)
rno05145	Toxoplasmosis	P63018	Heat shock cognate 71 kDa protein (9)
rno05162	Measles	P63018	Heat shock cognate 71 kDa protein (9)
rno05164	Influenza A	P63018	Heat shock cognate 71 kDa protein (9)
rno04360	Axon guidance	P45592	Cofilin-1 (4)
rno04666	Fc gamma R-mediated phagocytosis	P45592	Cofilin-1 (4)
rno04810	Regulation of actin cytoskeleton	P45592	Cofilin-1 (4)
rno05133	Pertussis	P45592	Cofilin-1 (4)
rno04260	Cardiac muscle contraction	P16409	Myosin light chain 3 (3)
rno05410	Hypertrophic cardiomyopathy (HCM)	P16409	Myosin light chain 3 (3)
rno05414	Dilated cardiomyopathy	P16409	Myosin light chain 3 (3)
rno00230	Purine metabolism	P36972	Adenine phosphoribosyltransferase (2)
rno01100	Metabolic pathways	P36972	Adenine phosphoribosyltransferase (2)
rno03060	Protein export	P06761	78 kDa glucose-regulated protein (4)
rno05020	Prion diseases	P06761	78 kDa glucose-regulated protein (4)
rno03013	RNA transport	Q5RKI1	Eukaryotic initiation factor 4A-II (1)
		OR	OR
		Q6P3V8	Eukaryotic translation initiation factor 4A1 (1)
rno03320	PPAR signaling pathway	P07483	Fatty acid-binding protein (1)

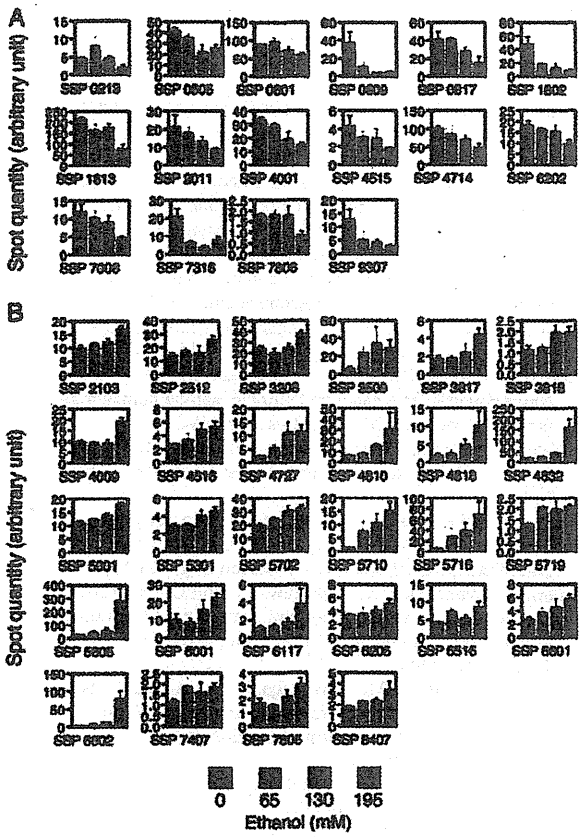

Fig. 3. Quantification of protein spots with expression changes in two-dimensional electrophoresis gels from rat embryos cultured in the presence of ethanol. Intensities of protein spots with ethanol-induced expression changes are shown. A. Protein spots with decreased intensity. B. Protein spots with increased intensity. Error bars indicate the standard error of the mean.

tein (standard spot numbers (SSPs) 4810, 4818), cofilin-1 (SSP 6001), and serum albumin (SSPs 4832, 5805, 6802), were the same as those identified as candidate proteins involved in embryotoxicity in our previous studies (Usami *et al.*, 2009, 2008); cofilin-1, which was increased, was found to be in its phosphorylated form.

Several protein spots were identified as charge variant forms of the same proteins, i.e., protein disulfide isomerase A3 (PDIA3; SSPs 4714, 4727, 5702, 5710, 5716, 6601), alpha-fetoprotein (SSPs 4810, 4818), and serum albumin (SSPs 4832, 5805, 6802). The quantities of spots that were identified as PDIA3 were increased (SSPs 4727, 5702, 5710, 5716, 6601), as well as decreased (SSP 4714) (Fig. 3). Because the PDIA3 spot with decreased quantity was the most acidic spot, it appeared that a basic pI shift of PDIA3 occurred in the groups exposed to ethanol.

Classification and mapping of proteins with ethanol-induced expression changes

According to their GO terms, the identified proteins were classified into various categories; the six major categories were "metabolism" (including 32% of the GO terms), "protein metabolism" (13%), "death" (9%), "developmental processes" (9%), "cell organization and biogenesis" (8%), and "stress response" (8%).

The identified proteins were mapped to 22 pathways using the KEGG pathway mapper (Table 4). Multiple proteins, i.e., PDIA3, 78-kDa glucose-regulated protein (SSP 1802), and heat shock cognate 71-kDa protein (SSP 1813), were mapped to the same two pathways, i.e., "protein processing in endoplasmic reticulum" (rno04141) and "antigen processing and presentation" (rno04612). Some proteins were mapped to multiple pathways, e.g., heat shock cognate 71-kDa protein (nine pathways), 78-kDa glucose-regulated protein (four pathways), and cofilin-1 (four pathways).

DISCUSSION

As mechanisms of ethanol-induced embryotoxicity, oxidative stress, and inhibited retinoid synthesis have been proposed (Goodlett *et al.*, 2005), which seems to be in accordance with the GO classification (32% metabolism and 8% stress response) of the proteins identified in the present study. In this context, expression changes in PDIA3 (also known as GRp58 and ERp57) are intriguing because it is an endoplasmic reticulum stress protein with oxidoreductase activity that regulates cellular redox homeostasis (Frickel *et al.*, 2004; Ni and Lee, 2007). PDIA3 is also involved in the nuclear translocation of retinoic acid receptor alpha (Zhu *et al.*, 2010) and its deficiency is embryonic lethal (Coe *et al.*, 2010). The identified proteins with GO terms classified into "death" may be involved in ethanol-induced apoptosis of neuronal cells, which has frequently been observed (Ahlgren *et al.*, 2002; Giles *et al.*, 2008). The present results also agreed with some biological networks that were perturbed by ethanol in cultured whole mouse embryos, involving cell death, reproductive system and antigen processing (Mason *et al.*, 2012). The pathways associated with multiple identified proteins may be more susceptible to ethanol, because these pathways could be affected at multiple steps simultaneously. On the other hand, the finding that

multiple pathways were associated with the same proteins might partially explain the complexity of ethanol-induced embryotoxicity.

ACKNOWLEDGMENT

This work was supported by a Health and Labor Science Research Grant from the Ministry of Health, Labor and Welfare in Japan.

REFERENCES

Ahlgren, S.C., Thakur, V. and Bronner-Fraser, M. (2002): Sonic hedgehog rescues cranial neural crest from cell death induced by ethanol exposure. Proc. Natl. Acad. Sci. USA, **99**, 10476-10481.

Chen, H., Boontheung, P., Loo, R.R., Xie, Y., Loo, J.A., Rao, J.Y. and Collins, M.D. (2008): Proteomic analysis to characterize differential mouse strain sensitivity to cadmium-induced forelimb teratogenesis. Birth Defects Res. A Clin. Mol. Teratol., **82**, 187-199.

Coe, H., Jung, J., Groenendyk, J., Prins, D. and Michalak, M. (2010): ERp57 modulates STAT3 signaling from the lumen of the endoplasmic reticulum. J. Biol. Chem., **285**, 6725-6738.

Frickel, E.-M., Frei, P., Bouvier, M., Stafford, W.F., Helenius, A., Glockshuber, R. and Ellgaard, L. (2004): ERp57 is a multifunctional thiol-disulfide oxidoreductase. J. Biol. Chem., **279**, 18277-18287.

Giavini, E., Broccia, M.L., Prati, M., Bellomo, D. and Menegola, E. (1992): Effects of ethanol and acetaldehyde on rat embryos developing *in vitro*. Vitr. Cell. Dev. Biol., **28A**, 205-210.

Giles, S., Boehm, P., Brogan, C. and Bannigan, J. (2008): The effects of ethanol on CNS development in the chick embryo. Reprod. Toxicol., **25**, 224-230.

Goodlett, C.R., Horn, K.H. and Zhou, F.C. (2005): Alcohol teratogenesis: mechanisms of damage and strategies for intervention. Exp. Biol. Med., **230**, 394-406.

Groebe, K., Hayess, K., Klemm-Manns, M., Schwall, G., Wozny, W., Steemans, M., Peters, A.K., Sastri, C., Jaeckel, P., Stegmann, W., Zengerling, H., Schopf, R., Poznanovic, S., Stummann, T.C., Seiler, A., Spielmann, H. and Schrattenholz, A. (2010): Protein biomarkers for *in vitro* testing of embryotoxicity. J. Proteome Res., **9**, 5727-5738.

Hu, Z.-L., Bao, J. and Reecy, J.M. (2008): CateGOrizer: A web-based program to batch analyze gene ontology classification categories. Online J. Bioinforma., **9**, 108-112.

Jain, E., Bairoch, A., Duvaud, S., Phan, I., Redaschi, N., Suzek, B.E., Martin, M.J., McGarvey, P. and Gasteiger, E. (2009): Infrastructure for the life sciences: design and implementation of the UniProt website. BMC Bioinformatics, **10**, 136.

Li, H. and Kim, K.H. (2003): Effects of ethanol on embryonic and neonatal rat testes in organ cultures. J. Androl., **24**, 653-660.

Mason, S., Anthony, B., Lai, X., Ringham, H.N., Wang, M., Witzmann, F.A., You, J.-S. and Zhou, F.C. (2012): Ethanol exposure alters protein expression in a mouse model of fetal alcohol spectrum disorders. Int. J. Proteomics, **2012**, 867141.

Ni, M. and Lee, A.S. (2007): ER chaperones in mammalian development and human diseases. FEBS Lett., **581**, 3641-3651.

Szabo, G., Puppolo, M., Verma, B. and Catalano, D. (1994): Regulatory potential of ethanol and retinoic acid on human monocyte functions. Alcohol. Clin. Exp. Res., **18**, 548-554.

UniProt Consortium (2011): Ongoing and future developments at the Universal Protein Resource. Nucleic Acids Res., **39**, D214-219.

Usami, M. and Mitsunaga, K. (2011): Proteomic analysis and *in vitro* developmental toxicity tests for mechanism-based safety evaluation of chemicals. Expert Rev. Proteomics, **8**, 153-155.

Usami, M., Mitsunaga, K., Nakazawa, K. and Doi, O. (2008): Proteomic analysis of selenium embryotoxicity in cultured postimplantation rat embryos. Birth Defects Res. B Dev. Reprod. Toxicol., **83**, 80-96.

Usami, M., Nakajima, M., Mitsunaga, K., Miyajima, A., Sunouchi, M. and Doi, O. (2009): Proteomic analysis of indium embryotoxicity in cultured postimplantation rat embryos. Reprod. Toxicol., **28**, 477-488.

Wentzel, P. and Eriksson, U.J. (2008): Genetic influence on dysmorphogenesis in embryos from different rat strains exposed to ethanol *in vivo* and *in vitro*. Alcohol. Clin. Exp. Res., **32**, 874-887.

Zhou, F.C., Zhao, Q., Liu, Y., Goodlett, C.R., Liang, T., McClintick, J.N., Edenberg, H.J. and Li, L. (2011): Alteration of gene expression by alcohol exposure at early neurulation. BMC Genomics, **12**, 124.

Zhu, L., Santos, N.C. and Kim, K.H. (2010): Disulfide isomerase glucose-regulated protein 58 is required for the nuclear localization and degradation of retinoic acid receptor alpha. Reproduction, **139**, 717-731.

Congenital Anomalies
THE JAPANESE TERATOLOGY SOCIETY
doi:10.1111/cga.12036
Congenital Anomalies 2014; **54**, 67–68

LETTER TO THE EDITOR

Various definitions of reproductive indices: A proposal for combined use of brief definitions

Several reproductive indices, such as live birth index, are calculated as endpoints to be evaluated in toxicity tests concerning reproductive effects of chemicals. These indices are useful to correct for variations resulting from infertility and multiple pregnancy, for example, the varied numbers of pups, among treatment groups and dams, respectively. In the toxicity test reports, the reproductive indices are used with their definitions, usually expressed as calculation formulae, to describe what they mean.

Despite their frequent use, however, the definitions of the reproductive indices have not been standardized; that is, they are different among laboratories, and are confusing. For example, the live birth index is "number of live newborns/number of implantation sites × 100" in some laboratories, but is "number of live newborns/number of total newborns × 100" in others, as listed in Table 1. These two definitions are quite different from each other in that the latter does not involve postimplantation loss, but the former does, though the live birth index is one of the most important reproductive indices. In most toxicity test laboratories, on the other hand, the definitions of reproductive indices cannot be changed even for standardization because they are defined as a part of laboratory computer systems.

In the database era, the confusion of reproductive indices has become more serious than ever, because data from various laboratories in the toxicity databases are frequently consulted at a time as in meta-analyses for building quantitative structure-activity relationship models. In the meta-analysis of reproductive toxicity data, reproductive indices cannot be used as toxicological endpoints to be evaluated unless their definitions, usually not found in the abstract because of their lengthiness, are clearly identified.

As a solution to this issue, we here propose combined use of brief definitions that describe the meaning of the reproductive indices with simpler words than the calculation formulae, for example, "live newborn/nidation rate" for "number of live newborns/number of implantation sites × 100." Explanatory descriptions of the reproductive indices with their brief definitions, for example, "the live birth index (live newborn/nidation rate)" at their first appearance in the abstract and main text would be most helpful.

In this letter, we show various definitions of representative reproductive indices and propose their brief definitions. We found 14 reproductive indices with 23 definitions by a brief survey of toxicological reference books (Manson and Kang 1989; Mizutani 1992; Saikikeisei ni kansuru dejitaruka sagyogruupu iinkai 1994; Econbichon 1995; Parker 2012) and contract research organizations' reports in a toxicological database (Japan Existing Chemical Data Base, http://dra4.nihs.go.jp/mhlw_data/jsp/SearchPage.jsp). From these indices, we show seven representative indices and 12 brief definitions as examples (Table 1), but it is not intended that the brief definitions presented here should be used as they are.

Correspondence: Makoto Usami, PhD, Division of Pharmacology, National Institute of Health Sciences, 1-18-1, Setagaya, Tokyo 158-8501, Japan. Email: usami@nihs.go.jp

Received August 28, 2013; revised and accepted October 29, 2013.

Makoto Usami[1], Katsuyoshi Mitsunaga[2], Tomohiko Irie[1], and Mikio Nakajima[3]

[1]Division of Pharmacology, National Institute of Health Sciences, Tokyo, [2]School of Pharmaceutical Sciences, Toho University, Chiba, and [3]Pharmaceuticals Research Center, Asahi Kasei Pharma Corporation, Shizuoka, Japan

REFERENCES

Econbichon DJ. 1995. Reproductive toxicology. In: Derelanko MJ, Hollinger MA, editors. CRC handbook of toxicology. Boca Raton: CRC Press. p 379–402.

Manson JM, Kang YJ. 1989. Test methods for assessing female reproductive and developmental toxicology. In: Hayes AW, editor. Principles and methods of toxicology, 2nd edn. New York: Raven Press, Ltd. p 311–359.

Mizutani M. 1992. Seisyoku hassei dokusei no jissai. In: Tanimura T, editor. Developmental toxicology. Tokyo: Chijinshokan. p 143–167. (In Japanese.)

Parker RM. 2012. Reproductive toxicity testing-Methodology. In: Hood RD, editor. Developmental and reproductive toxicology: a practical approach, 3rd edn. London: Informa Healthcare. p 184–228.

Saikikeisei ni kansuru dejitaruka sagyogruupu iinkai. 1994. Saikikesei Yogo. In: Nakadate M, editor. Toxicity testing. Tokyo: National Institute of Health Sciences, Biological Safety Research Center. p 394–488. (In Japanese.) Available at URL: http://www.nihs.go.jp/center/yougo/saiki.html.

Table 1 Representative reproductive indices and their definitions appeared in reference books and toxicity reports

	Definition†									
	Reference Book					Contract research organization's reproductive toxicity test report				
Reproductive index	Manson & Kang, 1989	*Mizutani, 1992*	*Ecobichon, 1995*	*Saikikeisei. 1994*	Parker. 2012	*Laboratory A*	*Laboratory B*	*Laboratory C*	*Laboratory D*	Example of brief definition
Implantation index					Implants/Corpora lutea	Implantation sites/ Corpora lutea	Implantation sites/ Corpora lutea	Implantation scars/ Corpora lutea	Implantation sites/ Corpora lutea	Nidation/luteum rate
			Implantations/Pregnant females							Nidation/pregnant rate
Gestation index		*Females with live* offspring/Pregnant females		*Females with live* offspring/Pregnant females	*Females with live* born/Females with evidence of pregnancy	*Females with live pups*/ Pregnant females				*Live delivered* dam/pregnant rate
Delivery index							Females which delivered live borns/ Pregnant females	Dams with live offspring/Pregnant dams	Pregnant females with live pups at birth/ Pregnant females	
		Pups born/Implantation sites				Pups born/Implantation sites		Offspring at birth/ Implantation scars	Pups born/Implantation sites	Newborn/nidation rate
Live birth index			(Viable pups born/ litter)/(Pups born/ litter)		Pups born alive/Total pups born	Live pups on lactation day 0/Pups born		Live offspring at birth/ Offspring at birth	Live pups at birth/Pups born	Live/total newborn rate
	Pups alive day 1/Pups born alive									Day 1 live pup/live newborn rate
		Live born/Implantation sites					Live born/Implantation sites			Live newborn/ nidation rate
Birth index				Offspring born alive/ Implantations				Live offspring at birth/ Implantation scars	Live pups at birth/ Implantation sites	
Viability index		Offspring alive on day 4 after birth/Live born		Offspring alive on day 4 after birth/Offspring *born alive*		Live pups on lactation day 4/Live pups on lactation day 0	Live pups on postnatal day 4/Live born	Live offspring at 4 days after birth/Live *offsprings at birth*	Live pups on postnatal day 4/Live pups at birth	Day 4 live pup/live newborn rate
	Pups alive day 7/Pups alive day 1									Days x/y live/live pup rate
			Viable pups born/Dead pups born							Live/dead newborn rate
Sex ratio (at birth)			Male offspring/Female offspring		Male offspring/Total offspring	Male pups born/Pups born		Male offspring/(Male offspring + female offspring)	Males born/Pups born	Male/total pup rate
						Live male pups/Live pups	Live born males/Live born			Live male /live total pup rate

†Common descriptions, "number of" and "× 100," are omitted.

Congenital Anomalies
THE JAPANESE TERATOLOGY SOCIETY
184 *Congenital Anomalies* 2014; **54**, 184–188 doi:10.1111/cga.12059

SHORT COMMUNICATION

Simple *in vitro* migration assay for neural crest cells and the opposite effects of all-*trans*-retinoic acid on cephalic- and trunk-derived cells

Makoto Usami[1], Katsuyoshi Mitsunaga[2], Tomohiko Irie[1], Atsuko Miyajima[3], and Osamu Doi[4]
Divisions of [1]Pharmacology and [3]Medical Devices, National Institute of Health Sciences, Tokyo, [2]School of Pharmaceutical Sciences, Toho University, Chiba, and [4]Laboratory of Animal Reproduction, United Graduate School of Agricultural Science, Gifu University, Gifu, Japan

ABSTRACT **Here, we describe a simple *in vitro* neural crest cell (NCC) migration assay and the effects of all-*trans*-retinoic acid (RA) on NCCs. Neural tubes excised from the rhombencephalic or trunk region of day 10.5 rat embryos were cultured for 48 h to allow emigration and migration of NCCs. Migration of NCCs was measured as the change in the radius (radius ratio) calculated from the circular spread of NCCs between 24 and 48 h of culture. RA was added to the culture medium after 24 h at embryotoxic concentrations determined by rat whole embryo culture. RA (10 μM) reduced the migration of cephalic NCCs, whereas it enhanced the migration of trunk NCCs, indicating that RA has opposite effects on these two types of NCCs.**

Key Words: developmental toxicity, embryo, migration assay, neural crest cell, rat

INTRODUCTION

In vertebrate development, neural crest cells (NCCs) migrate from the neural primordia throughout the embryo and contribute to morphogenesis (Douarin and Kalcheim 1999). Malfunction of NCCs leads to dysmorphologies, tumors, and syndromes called neurocristopathies (Hall 2009). In developmental toxicology, it has been proposed that altered migration of cephalic NCCs induced by chemicals leads to fetal malformation. For example, retinoic acids and fluconazole inhibited the migration of cephalic NCCs, causing branchial abnormalities in cultured rat and mouse embryos (Pratt et al. 1987; Menegola et al. 2004). These abnormalities are considered to result in *in vivo* craniofacial malformations, such as the cleft palate, cleft lip, micrognathia, and thymic agenesis (Hall 2009).

However, the effects of developmental toxicants on the migration of NCCs in mammals have not been fully investigated because no convenient experimental methods are available. Migration of NCCs is usually examined by time-lapse video imaging of *in vitro* cultured cells (Fuller et al. 2002) or *in vivo* fluorescently labeled cells (Kawakami et al. 2011). These methods are time-consuming and are not suitable for developmental toxicity investigations of chemicals.

In the present study, we have described a simple migration assay that enables investigation of the effects of chemicals on rat NCCs. Cephalic or trunk NCCs were cultured as emigrants from isolated neural tubes of day 10.5 rat embryos. The cultured NCCs were exposed to test chemicals for 24 to 48 h, and their migration was determined as the change in the radius calculated from the circular spread of the NCCs during exposure. By using this assay method, we found that RA has opposite effects on the migration of cephalic and trunk NCCs.

Correspondence: Makoto Usami, PhD, Division of Pharmacology, National Institute of Health Sciences, 1-18-1, Kamiyoga, Setagaya, Tokyo 158-8501, Japan. Email: usami@nihs.go.jp

Received January 8, 2014; revised and accepted March 31, 2014.

MATERIALS AND METHODS

Animals

Wistar rats (Crj:WI; Charles River Japan, Kanagawa, Japan) were used in these assays. Pregnant rats were obtained by mating female and male rats overnight, and the plug day was designated as day 0.5 of gestation. All the animal experiments were performed in accordance with the guidelines for animal experiments of the National Institute of Health Sciences.

Rat whole embryo culture

Rat embryos on day 10.5 of gestation were cultured for 24 h by the roller bottle method as described previously (Usami et al. 2008). All-*trans*-retinoic acid (RA, CAS 302-79-4; Wako Pure Chemical Industries, Osaka, Japan) was dissolved in dimethyl sulfoxide before adding it to the culture medium, which was rat serum. Control embryos were cultured in the presence of the same concentration of dimethyl sulfoxide.

NCC culture

Neural crest cells were cultured as emigrated cells from the neural tubes of day 10.5 rat embryos, as outlined in Figure 1A. Neural tubes were excised from the rhombencephalic or trunk region of the embryos in Hanks' balanced salt solution with sharpened tungsten needles. The excised neural tubes (approximately 0.7 mm long) were cut open dorsally and attached to the 35-mm culture dishes (BD Primaria; Becton Dickinson, Franklin Lakes, NJ, USA) containing 2 mL of Dulbecco's Modified Eagle Medium with high glucose (DMEM; Gibco, Life Technologies, Carlsbad, CA, USA) and 10% (v/v) fetal bovine serum (Gibco) (Fig. 1B,C). The dishes were incubated at 37°C with 5% CO_2 for 48 h. After 24 h of culture, the medium was replaced with medium containing RA dissolved in dimethyl sulfoxide (final concentration, 0.1% v/v).

Observation and analysis of cultured NCCs

Neural crest cells emigrated from the neural tubes were observed for their attachment to the surface of the culture vessels and the extent of migration. Images of cultured NCCs were recorded digitally with a phase-contrast microscope (BZ-9000; Keyence, Osaka, Japan) after 24 and 48 h of culture. NCCs that did not completely surround the neural tube after 24 h of culture and those cultures in

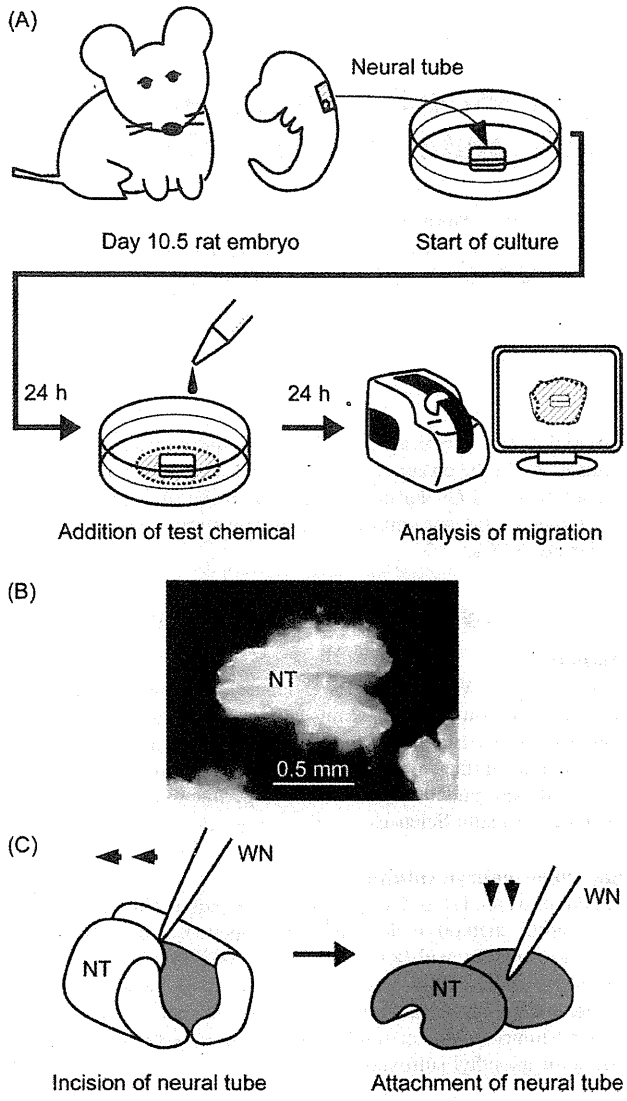

Fig. 1 Outline of the neural crest cell (NCC) migration assay. (A) Neural tubes were excised from the rhombencephalic region of day 10.5 rat embryos and cultured for 48 h to allow emigration of the NCCs. Test chemicals were added to the culture medium after 24 h of culture. Migration indices were calculated as the circular spread of NCCs after 24 and 48 h of culture. (B) A dorsal view of a neural tube prepared for culture. The right side is cranial. (C) Neural tubes were incised dorsally and pressed to the culture plate surface with the outer wall downward using a tungsten needle. It should be noted that the neural tubes became concave outward after the incision. NT, neural tube. WN, tungsten needle.

which the neural tube detached from the surface of the culture vessel before the end of the culture period were omitted from the analyses because they showed little migration.

The migration distance of the NCCs was calculated as the increase in the radius of the circular spread between 24 and 48 h of culture. The digital images of cultured NCCs were analyzed by using ImageJ software (http://rsb.info.nih.gov/ij/, 1997–2009; Rasband, W.S., ImageJ, U. S. National Institutes of Health, Bethesda, MD, USA). The outermost NCCs in each of the cultured neural tubes were connected with the polygon tool as if a rubber band were placed around the cells, and the pixel count inside the polygon was measured. Considering the polygon as a circle, its radius was calculated as follows:

$$\text{Radius} = \sqrt{(\text{number of pixels in polygon}/\pi)}.$$

To assess NCC migration, the radius ratio was calculated using the following formula:

$$\text{Radius ratio} = (\text{radius at 48 h} - \text{radius at 24 h})/\text{radius at 24 h}.$$

This ratio was then normalized to the control to allow for comparisons between experiments.

Immunocytochemistry

At the end of the culture period, the neural tubes and non-NCCs derived from surrounding tissues were removed with tungsten needles under a stereomicroscope, leaving the emigrated cells in the dish. The emigrated cells were fixed with 4% (w/v) paraformaldehyde in phosphate-buffered saline (PBS) for 20 min, permeated with 0.1% Triton X-100 in PBS for 2 min, and blocked with 3% (w/v) bovine serum albumin (BSA) in PBS for 30 min at room temperature. The treated cells were incubated with a primary antibody in 1% (w/v) BSA-PBS for 1 h, and then incubated with a secondary antibody in 1% (w/v) BSA-PBS for 1 h at room temperature. The primary antibodies used were an anti-HNK-1 mouse IgM monoclonal antibody (CBL519; Merck KGaA, Darmstadt, Germany) and an anti-SOX10 mouse IgG monoclonal antibody (MAB2864; R & D Systems, Minneapolis, MN), and the secondary antibodies used were fluorescently labeled anti-mouse (Alexa Fluor 488 goat anti-mouse IgM, A-21042; Invitrogen, Life Technologies) and anti-rabbit (Alexa Fluor 594 goat anti-mouse IgG (H + L), A-11005; Invitrogen) antibodies. To stain the cell nuclei, 4',6-diaminodino-2-phenylindole (DAPI, D-1306; Invitrogen) dissolved in methanol (2 mg/mL) was added to the secondary antibody solutions at a concentration of 0.1% (v/v). The immunostained cells were photographed with a fluorescence microscope (BZ-9000, equipped with the DAPI-BP, GFP-BP, and Texas Red filters; Keyence).

Statistical analysis

Statistical significance of the difference between the experimental groups was examined by the Student's *t*-test or Fisher's exact test.

RESULTS

Identification of NCCs

Cells emigrated from explanted rhombencephalic and trunk neural tubes during culture were identified as NCCs by immunocytochemistry of the following marker antigens, HNK-1 (Nagase et al. 2003) on the cell membrane and SOX10 (Kim et al. 2003) in the cell nucleus. The nuclei of the emigrated cells were stained by DAPI and the anti-SOX10 antibody, and the cells were stained by the anti-HNK-1 antibody (Fig. 2A–C). The merged images showed the co-expression of HNK-1 and SOX10 in the emigrated cells at least in the periphery of the circular spread (Fig. 2D). Thus, the emigrated cells were identified as NCCs.

Analysis of NCC migration

Figure 3A shows images of NCCs after 24 and 48 h of culture. The migration of NCCs was calculated as the difference in the radius of the circular spread of the cells between 24 and 48 h of culture because it was impossible to determine the migration distance from

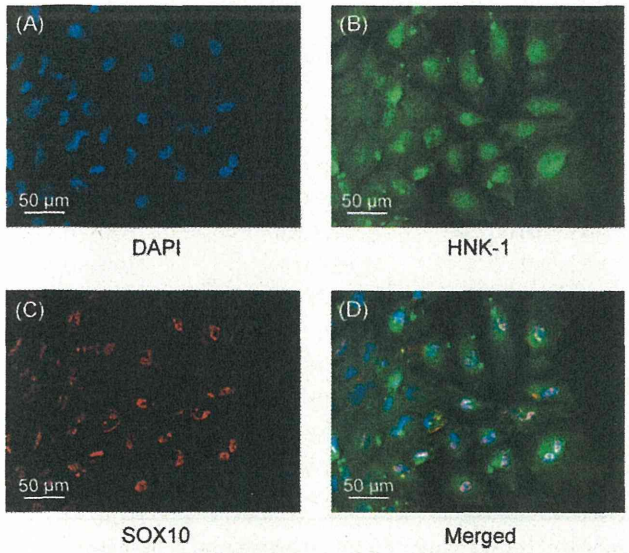

Fig. 2 Immunocytochemical identification of neural crest cells (NCCs). (A) Nuclear staining with 4′6′-diamidino-2-phenylindole dihydrochloride (DAPI). (B) Staining of the cell membrane with an anti-HNK-1 antibody. (C) Staining of nuclei with an anti-SOX10 antibody. (D) A merged image of A, B, and C.

the neural tube since its outline was obscured during culture, and individual NCCs could not be distinguished. The mean migration distance of the NCCs calculated using this method was approximately 500 μm during the 24-h culture period. To evaluate NCC migration, the radius ratio was used because this ratio showed less variability than the radius difference as determined by the coefficient of variation, suggesting the dependence of NCC migration on the size of the explanted neural tubes (Fig. 3B).

Effects of RA on cultured rat embryos

Embryotoxic concentrations of RA were determined by rat whole embryo culture to compare RA-induced embryotoxicity to the effects of RA on NCC migration. RA was toxic to cultured rat embryos at concentrations ≥3 μM, which caused a reduction in the number of somite pairs and an increased incidence of morphological abnormalities (Table 1). Deformed branchial arches, more specifically, the hypoplastic 3rd branchial arch, were observed at 10 μM RA but not at 3 μM (Fig. 4). These embryotoxic concentrations were comparable to those in the maternal plasma (about 4.5 μg/mL = 15 μM) obtained by the administration of a teratogenic dose (10 mg/kg) of RA to mice (Kraft 1992), and the observed abnormalities corresponded to *in vivo* malformations of the ear, eye, and thymus. Based on these results, RA was added at 0, 3, and 10 μM during the 24-h exposure period in the following NCC migration experiments.

Effects of RA on NCC migration

Rat NCCs emigrated from the neural tube were exposed to embryotoxic concentrations of RA for 24 h. RA reduced the migration of cephalic NCCs in a concentration dependent manner, and 10 μM RA reduced the migration by approximately 10% (Fig. 5A). In contrast, RA (10 μM) enhanced the migration of trunk NCCs by

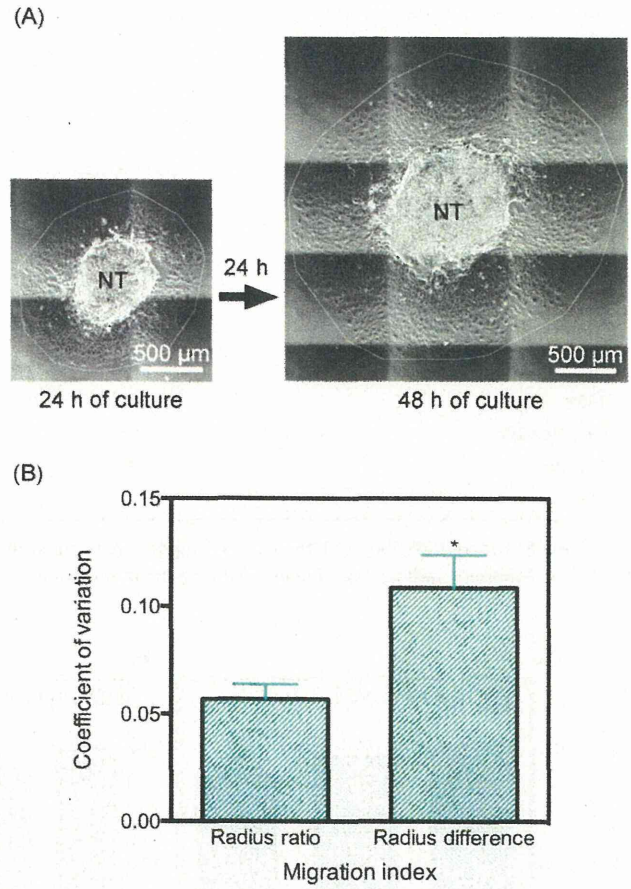

Fig. 3 Analysis of neural crest cell (NCC) migration. (A) Cultured NCCs were enclosed in a polygon to calculate the migration indices after 24 and 48 h of culture. (B) Comparison of migration indices. The means ± standard error of the mean (SEM) of the coefficient of variation from eight control cultures are shown for the migration indices: the radius ratio and the radius difference.

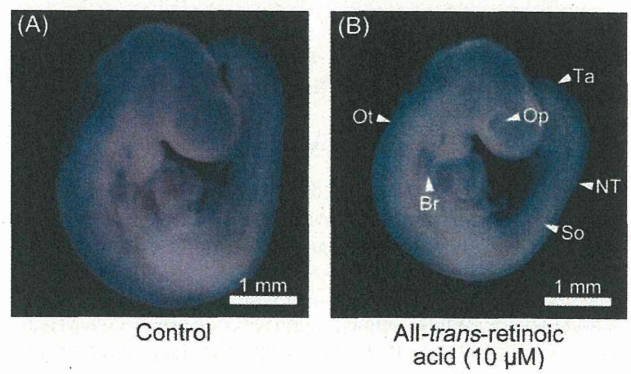

Fig. 4 Appearance of rat embryos cultured in the presence of all-*trans*-retinoic acid. Rat embryos after 24 h of culture are shown after removal of the embryonic membranes. Arrowheads indicate deformed organs. Br, branchial arch; NT, neural tube; Op, optic vesicle; Ot, otic vesicle; So, somite; Ta, tail.

Table 1 Growth of day 10.5 rat embryos cultured in the presence of all-*trans*-retinoic acid (RA)

	All-*trans*-retinoic acid (μM)			
	0 (Control)	1	3	10
No. embryos	6	6	6	6
No. viable embryos	6 (100%)	6 (100%)	6 (100%)	5 (83.3%)
Crown-rump length (mm)	4.28 ± 0.05	4.45 ± 0.07	4.29 ± 005	4.12 ± 0.22
Head length (mm)	2.34 ± 0.04	2.40 ± 0.04	2.34 ± 0.06	2.19 ± 0.13
No. somite pairs	27.7 ± 0.21	27.5 ± 0.22	27.0 ± 0.37	25.6 ± 0.60**
No. embryos with deformed organ	0	0	5 (83.3%)**	5 (100%)**
Branchial arch	0	0	0	4 (80.0%)*
Neural tube	0	0	5 (83.3%)**	5 (100%)**
Optic vesicle	0	0	5 (83.3%)**	4 (80.0%)*
Otic vesicle	0	0	5 (83.3%)**	5 (100%)**
Somite	0	0	2 (33.3%)	3 (60.0%)
Tail	0	0	2 (33.3%)	1 (20.0%)

Embryos were cultured for 24 h by the roller method in the medium composed of pure rat serum. Mean ± standard error of the mean (SEM) is shown. Asterisks indicate significant difference from the control value (*$P < 0.05$; **$P < 0.01$).

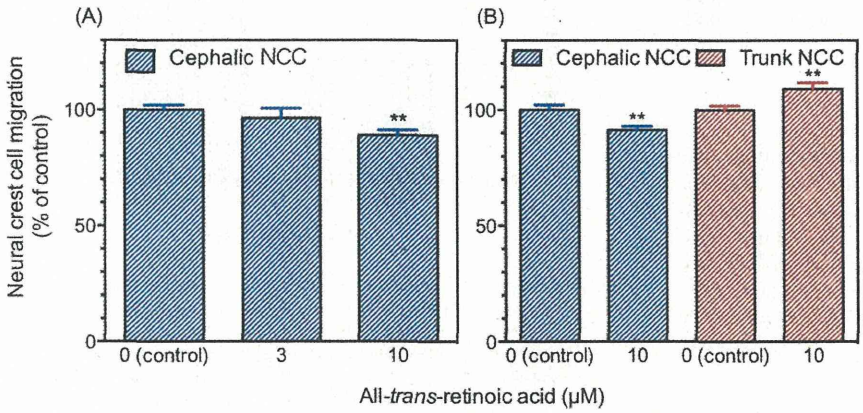

Fig. 5 Neural crest cell (NCC) migration during 24 h of culture in the presence of all-*trans*-retinoic acid (RA). (A) Effects of RA on cephalic NCCs. (B) Effects of RA on trunk NCCs. NCC migration was calculated as the ratio of the radius from the circular spread of the NCCs and was normalized to the control. The means ± standard error of the mean (SEM) of 9–11 neural tubes are shown. Asterisks indicate statistically significant differences from the corresponding control (**$P < 0.01$).

approximately 10%, indicating the RA has opposite effects on cephalic and trunk NCCs (Fig. 5B).

DISCUSSION

In the present study, we established a simple *in vitro* NCC migration assay that enabled easy assessment of the effects of chemicals on NCC migration in developmental toxicity studies. However, the present method is not suitable for screening because the concentrations found to be effective do not provide information on overall embryotoxicity. Whole embryo culture or general cytotoxicity assays in combination with the present NCC migration assay should be useful for examining the specific effects of chemicals on NCCs. One advantage of the present NCC migration assay is that general cellular techniques and toxicogenomic analyses for toxicological mechanistic studies are easily applicable to NCCs isolated by the removal of neural tubes, as described for the immunocytochemistry methodology.

By using this method, we found that RA had opposite effects on the migration of cephalic and trunk NCCs. The reduction in cephalic NCC migration induced by RA is consistent with previous reports that described the inhibitory effects of RA on cephalic NCCs as a pathogenic mechanism underlying craniofacial malformation (Pratt et al. 1987; Menegola et al. 2004). In the present study, we observed hypoplasia of the 3rd branchial arch, the formation of which is dependent on migrated cephalic NCCs, at the same RA concentration that reduced cephalic NCC migration. Enhancement of trunk NCC migration is not directly related to any known developmental toxicity of RA. However, these opposite effects on cephalic and trunk NCCs will make it easy to investigate the mechanisms underlying RA effects on NCCs by allowing comparative analysis.

When evaluating the results of the present NCC migration assay, it should be noted that altered migration is not necessarily a direct effect of the chemical on the motility of NCCs. Because NCC migration in the present assay was determined as the circular spread of the cells, the number of cells can influence the result, that is, a decrease in the number of cells induced by cytotoxicity can result in a reduced migration index. It is also possible that altered NCC migration is due to the effects of chemicals on the neural tube. This

is because NCC migration in the present assay is dependent on the presence of a neural tube, as evidenced by the reduced migration of NCCs whose neural tube detached from the culture surface.

In conclusion, we established a simple migration assay that enables investigation of the effects of chemicals on rat NCCs. By using this assay method, we found that RA has opposite effects on the migration of cephalic and trunk NCCs.

ACKNOWLEDGMENTS

This work was supported by a Health and Labor Science Research Grant from the Ministry of Health, Labor, and Welfare of Japan.

CONFLICT OF INTEREST

The authors declare that there are no conflicts of interest.

REFERENCES

Douarin NL, Kalcheim C. 1999. The neural crest. 2nd edn. Vol. 9. New York: Cambridge University Press.

Fuller LC, Cornelius SK, Murphy CW, Wiens DJ. 2002. Neural crest cell motility in valproic acid. Reprod Toxicol 16:825–839.

Hall BK. 2009. Neurocristopathies. In: The neural crest and neural crest cells in vertebrate development and evolution, 2nd edn. New York: Springer. p 269–293.

Kawakami M, Umeda M, Nakagata N, Takeo T, Yamamura K-I. 2011. Novel migrating mouse neural crest cell assay system utilizing P0-Cre/EGFP fluorescent time-lapse imaging. BMC Dev Biol 11:68.

Kim J, Lo L, Dormand E, Anderson DJ. 2003. SOX10 maintains multipotency and inhibits neuronal differentiation of neural crest stem cells. Neuron 38:17–31.

Kraft J. 1992. Pharmacokinetics, placental transfer, and teratogenicity of 13-*cis*-retinoic acid, its isomer, and metabolites. In: Morriss-Kay GM, editor. Retinoids in normal development and teratogenesis. New York: Oxford University Press. p 267–280.

Menegola E, Broccia ML, Di Renzo F, Massa V, Giavini E. 2004. Relationship between hindbrain segmentation, neural crest cell migration and branchial arch abnormalities in rat embryos exposed to fluconazole and retinoic acid *in vitro*. Reprod Toxicol 18:121–130.

Nagase T, Sanai Y, Nakamura S, Asato H, Harii K, Osumi N. 2003. Roles of HNK-1 carbohydrate epitope and its synthetic glucuronyltransferase genes on migration of rat neural crest cells. J Anat 203:77–88.

Pratt RM, Goulding EH, Abbott BD. 1987. Retinoic acid inhibits migration of cranial neural crest cells in the cultured mouse embryo. J Craniofac Genet Dev Biol 7:205–217.

Usami M, Mitsunaga K, Nakazawa K, Doi O. 2008. Proteomic analysis of selenium embryotoxicity in cultured postimplantation rat embryos. Birth Defects Res B Dev Reprod Toxicol 83:80–96.